

Meta-generalized gradient approximations in time dependent generalized Kohn–Sham theory: Importance of the current density correction

Cite as: *J. Chem. Phys.* **159**, 124117 (2023); doi: [10.1063/5.0167972](https://doi.org/10.1063/5.0167972)

Submitted: 16 July 2023 • Accepted: 7 September 2023 •

Published Online: 28 September 2023



View Online



Export Citation



CrossMark

Rian Richter,  Thilo Aschebrock,  Ingo Schelter,  and Stephan Kümmel^{a)} 

AFFILIATIONS

Theoretical Physics IV, University of Bayreuth, 95440 Bayreuth, Germany

^{a)} Author to whom correspondence should be addressed: stephan.kuemmel@uni-bayreuth.de

ABSTRACT

We revisit the use of Meta-Generalized Gradient Approximations (mGGAs) in time-dependent density functional theory, reviewing conceptual questions and solving the generalized Kohn–Sham equations by real-time propagation. After discussing the technical aspects of using mGGAs in combination with pseudopotentials and comparing real-space and basis set results, we focus on investigating the importance of the current-density based gauge invariance correction. For the two modern mGGAs that we investigate in this work, TASK and r^2 SCAN, we observe that for some systems, the current density correction leads to negligible changes, but for others, it changes excitation energies by up to 40% and more than 0.8 eV. In the cases that we study, the agreement with the reference data is improved by the current density correction.

© 2023 Author(s). All article content, except where otherwise noted, is licensed under a Creative Commons Attribution (CC BY) license (<http://creativecommons.org/licenses/by/4.0/>). <https://doi.org/10.1063/5.0167972>

I. INTRODUCTION

Time-dependent density functional theory (TDDFT) is frequently used for calculating electronic excitations. The accuracy of a TDDFT calculation hinges on the approximation that is employed for the exchange–correlation (xc) functional. The local density approximation (LDA) and Generalized Gradient Approximations (GGAs) come at a low computational cost but suffer from systematic shortcomings that limit their usefulness. Functionals such as range-separated hybrids can be much more accurate, rivaling many-body perturbation theory and wavefunction methods in accuracy,^{1,2} yet they also come at a much higher numerical cost and conceptual complexity than semilocal functionals. In the context of ground-state density functional theory (DFT), meta-GGAs that depend on the non-interacting kinetic energy density have emerged as an attractive class of xc approximations with an accuracy better than GGAs,^{3–18} while still being semilocal in terms of the computational expense. Recently, it has been shown that a non-empirical construction strategy can give meta-GGAs that show (ultra-)nonlocality and can

describe static long-range charge-transfer in great similarity to Fock exchange,¹⁷ while also yielding reasonable results for many ground-state properties.¹⁹ This raises the hope that using meta-GGAs in TDDFT may allow us to overcome the systematic, qualitative failures of LDA and GGAs, without having to face the substantial increase in computational cost that is associated with fully non-local functionals.

Using a meta-GGA in TDDFT, however, is less straightforward than using explicit density functionals because the dependence on the kinetic energy density introduces a gauge dependence.^{20,21} In this paper, we revisit this issue and address it for two modern meta-GGAs, the r^2 SCAN¹⁸ and TASK¹⁷ functionals. In doing so, we rely on the real-time propagation formalism, which has been developed in different technical realizations in the past years.^{22–36} The real-time approach is finding increasing interest because, on the one hand, it allows us to go beyond the linear response regime and, on the other hand, it scales well with the system size³⁷ and can reach outstanding computational efficiency.

In Sec. II, we summarize the basic facts about meta-GGAs from the ground-state perspective, motivating why we focus on the r^2 SCAN and TASK functionals and discussing the technically relevant issue of using pseudopotentials in meta-GGA calculations. In Sec. III, we review the use of meta-GGAs in TDDFT and discuss the gauge variance problem and the current density correction that has been suggested to address it. Sections IV and V are devoted to the discussion of TDDFT meta-GGA results obtained with TASK and r^2 SCAN, respectively. We find that the current density correction can sometimes be small but can also have a significant impact and, therefore, should generally be taken into account when meta-GGAs are used in TDDFT. We close this paper with a summary and conclusions.

II. RECAPITULATING META-GGA CONCEPTS

In our work, we focus on two relatively recently developed meta-GGAs. One is the r^2 SCAN functional,¹⁸ which was derived from first-principles as a broadly applicable xc approximation that describes many different types of electronic bonding well, while defusing the numerical intricacies of the original SCAN construction¹⁴ to some extent. SCAN and r^2 SCAN are considered to be among the most accurate, non-empirical general-purpose meta-GGAs. However, here we can only report TDDFT results for r^2 SCAN and not SCAN because we could not reach a numerically long-term stable propagation with SCAN. This latter finding is no surprise (also see the comments in the supplementary material) in view of earlier reports about the numerical challenges associated with SCAN.^{18,38–41}

The second functional that we study is the TASK meta-GGA,¹⁷ which is also derived non-empirically from first-principles, fulfilling the same constraints on the exchange energy as SCAN, but with a focus on incorporating a realistic derivative discontinuity into the energy functional. This leads to a reliable prediction of bandgaps^{17,41,42} and, with a suitable correlation functional, also a reasonable accuracy for atomization energies and barrier heights.¹⁹

The exchange energies of both of these meta-GGAs can be written as an integral over the exchange energy density e_x^{mGGA} , i.e.,

$$E_x^{\text{mGGA}}[n] = \int e_x^{\text{mGGA}}(n, \nabla n, \tau) d^3r = A_x \int n^{4/3} F_x(s, \alpha) d^3r, \quad (1)$$

where $A_x = -(3e^2/4)(3/\pi)^{1/3}$, with e being the elementary charge, and $F_x(s, \alpha)$ is the enhancement factor, which depends on the following dimensionless variables:

$$s = \frac{|\nabla n|}{2(3\pi^2)^{1/3} n^{4/3}} \quad (2)$$

and

$$\alpha = \frac{\tau - \tau^W}{\tau^{\text{unif}}}. \quad (3)$$

Here,

$$n = \sum_{j=1}^N |\varphi_j|^2 \quad (4)$$

is the density and

$$\tau = \frac{\hbar^2}{2m} \sum_{j=1}^N |\nabla \varphi_j|^2 \quad (5)$$

is the kinetic energy density of the (generalized) Kohn–Sham system, where m denotes the electron mass. Finally,

$$\tau^W = \frac{\hbar^2}{8m} \frac{|\nabla n|^2}{n} \quad (6)$$

is the von Weizsäcker kinetic energy density and $\tau^{\text{unif}} = A_s n^{5/3}$, with $A_s = (3\hbar^2/10m)(3\pi^2)^{2/3}$ being the uniform density limit of τ .

A. Ground state generalized Kohn–Sham equations for meta-GGAs

As for any orbital-dependent density functional,⁴³ one has the choice of using mGGAs either in the Kohn–Sham scheme, i.e., with the potential calculated as the functional derivative with respect to the density in the optimized effective potential formalism, or in the generalized Kohn–Sham (GKS) scheme, i.e., calculating functional derivatives with respect to the orbitals. In TDDFT, meta-GGAs have been explored within the Kohn–Sham scheme, e.g., in the context of linear-response calculations that used the Sternheimer approach.⁴⁴ Here, however, we follow Refs. 21, 45, and 46 and focus on the GKS approach to avoid the serious difficulties^{26,47} that are associated with the solution of the time-dependent optimized effective potential equation, which could so far only be solved for one-dimensional model systems.^{48,49}

In contrast to Kohn–Sham theory, in which the real system is mapped to a non-interacting reference system, in GKS theory,⁴⁵ the mapping is to a partially interacting system with a ground state that is still a single Slater determinant Φ . Thus, the original formulation of GKS theory defined a functional $S[\Phi]$ that depends on a Slater determinant. However, for meta-GGAs, the dependence on the Slater determinant is not necessarily explicitly seen, yet it is important that S is a unitarily invariant functional of the occupied orbitals, $S[\{\varphi_k\}]$. The corresponding energy density functional $F^S[n]$ is then obtained from the orbitals that minimize S while yielding the density $n(\mathbf{r})$,

$$F^S[n] = \min_{\{\varphi_k\} \rightarrow n(\mathbf{r})} S[\{\varphi_k\}]. \quad (7)$$

One writes the meta-GGA energy functional as

$$S[\Phi] = \langle \Phi | T | \Phi \rangle + E_{xc}^{\text{mGGA}}[\{\varphi_k\}], \quad (8)$$

where $T = -\sum_{j=1}^N \frac{\hbar^2}{2m} \nabla_j^2$ and E_{xc}^{mGGA} depends on the set of occupied one-particle orbitals $\{\varphi_k\}$ in a unitarily invariant way via its dependence on n and τ . Taking the functional derivative with respect to the orbitals leads to the meta-GGA potential operator

$$\hat{v}^{\text{mGGA}} = v^{\text{loc}} + \hat{v}_\tau^{\text{GKS}}, \quad (9)$$

where

$$v^{\text{loc}} = \frac{\partial e_{xc}^{\text{mGGA}}}{\partial n} - \nabla \cdot \left[\frac{\partial e_{xc}^{\text{mGGA}}}{\partial (\nabla n)} \right] \quad (10)$$

is multiplicative as in a GGA and $\hat{v}_\tau^{\text{GKS}}$ is the differential operator,

$$\hat{v}_\tau^{\text{GKS}} = -\frac{\hbar^2}{2m} \nabla \cdot \frac{\partial e_{\text{xc}}^{\text{mGGA}}}{\partial \tau} \nabla, \quad (11)$$

with the meta-GGA xc energy density $e_{\text{xc}}^{\text{mGGA}}$. With the Hartree potential v_{H} as the “remainder potential,” one obtains the following GKS equation:

$$\left[-\frac{\hbar^2}{2m} \nabla^2 + v_{\text{ext}}(\mathbf{r}) + v_{\text{H}}[n](\mathbf{r}) + \hat{v}^{\text{mGGA}} \right] \varphi_k(\mathbf{r}) = \epsilon_k \varphi_k(\mathbf{r}), \quad (12)$$

with the external potential $v_{\text{ext}}(\mathbf{r})$ and the GKS eigenvalue ϵ_k .

B. Using pseudopotentials in meta-GGA calculations

In plane wave and real space calculations, the external potential in Eq. (12) is typically a pseudopotential that represents the interaction between the atomic cores and the valence electrons. In our calculations, we rely on the real-space code BTDF, which uses norm-conserving pseudopotentials of Troullier–Martins type.⁵¹ For orbital functionals, constructing consistent pseudopotentials is considerably more demanding than for semilocal functionals, such as LDA or GGAs, as demonstrated for exact exchange.^{43,52} First steps toward constructing pseudopotentials for meta-GGAs have been taken,⁵³ but including the differential operator part of the GKS potential, i.e., Eq. (11), into the pseudopotential construction is challenging, as the usual inversion from the pseudo-orbitals to the screened pseudopotential maps to a local potential. Thus, consistent pseudopotentials for r²SCAN and TASK are, unfortunately, not available yet. Using a non-consistent pseudopotential is always unsatisfactory from a formal point of view. In the context of exact exchange calculations, it has been demonstrated that the practical consequences of using a non-consistent pseudopotential need not necessarily be large.⁵⁴ However, in the context of meta-GGAs, special attention should, nevertheless, be devoted to the pseudopotential question because α of Eq. (3) (or the ratio τ^{W}/τ) is typically used to detect and adjust the meta-GGA to iso-orbital regions. A simple example demonstrates that the pseudopotential can have a significant influence on the iso-orbital character: In a sodium atom described by a usual LDA or GGA pseudopotential, which only treats the 3s electron as a valence electron, all of the valence density is iso-orbital and the meta-GGA treats xc effects in the Na atom as in the hydrogen atom. Meanwhile, in the all-electron calculation, the core electrons are present and the Na atom density is mostly not of iso-orbital character; thus, the meta-GGA does not switch to its iso-orbital limit. Consequently, a meta-GGA calculation for sodium based on a GGA pseudopotential may lead to very different results than a meta-GGA calculation based on all electrons. Thus, depending on the system that one studies, meta-GGAs can have a larger sensitivity to pseudopotential inconsistency than, for example, GGAs.

The problem, however, can be very much mitigated by adopting a technique that has been developed in Ref. 55 in the context of local hybrid functionals, which also use τ^{W}/τ for detecting iso-orbital regions. The key idea is that the core density is available in many pseudopotentials, e.g., for the purposes of the non-linear core correction,⁵⁶ and we can thus use the core density $n_{\text{c}}(\mathbf{r})$ in addition to the valence density $n_{\text{v}}(\mathbf{r})$ in the actual calculation to eliminate the

erroneous classification of the core region as an iso-orbital region. We achieve this by writing τ , τ^{W} , and τ^{unif} in Eq. (3) in the following forms:

$$\tau = \frac{\hbar^2}{2m} \left\{ \left(\sum_k^{\text{valence states}} |\nabla \varphi_k^{\text{v}}|^2 \right) + |\nabla(n_{\text{c}}(\mathbf{r}))^{1/2}|^2 \right\}, \quad (13)$$

$$\tau^{\text{W}} = \frac{\hbar^2}{8m} \frac{|\nabla(n_{\text{v}}(\mathbf{r}) + n_{\text{c}}(\mathbf{r}))|^2}{n_{\text{v}}(\mathbf{r}) + n_{\text{c}}(\mathbf{r})}, \quad (14)$$

$$\tau^{\text{unif}} = A_{\text{s}}(n_{\text{v}}(\mathbf{r}) + n_{\text{c}}(\mathbf{r}))^{5/3}, \quad (15)$$

where φ_k^{v} denotes the valence orbitals and

$$\sum_k^{\text{core states}} |\nabla \varphi_k(\mathbf{r})|^2 \approx |\nabla(n_{\text{c}}(\mathbf{r}))^{1/2}|^2 \quad (16)$$

has been used. The latter relation is exact for atoms with only one (doubly occupied) *s* core orbital. We have explicitly checked the accuracy of this procedure by comparing pseudopotential-based BTDF results with results obtained with the highly accurate all-electron code DARSEC^{57,58} for diatomic molecules.

For the calculations presented in Secs. IV and V, we can, therefore, be sure that the results for molecules that only consist of light atoms, such as N, C, O, and Li, e.g., CO and Li₂, are not at all affected by the pseudopotential iso-orbital problem. For molecules also containing atoms with more than just 1s core electrons, pseudopotentials with the core correction of Eq. (15) are used for the atoms with only a 1s core, whereas standard pseudopotentials are used for the heavier atoms. The comparison with all-electron calculations has shown that this pragmatic strategy leads to overall reliable results for the systems that we study in this paper. For general future work on meta-GGAs, consistent pseudopotentials are, of course, very desirable.

III. TIME-DEPENDENT GKS THEORY FOR META-GGAs

In the usual TD-GKS procedure, functionals are used in the orbital-adiabatic sense, i.e., the time-dependent orbitals are inserted into the potential expression that has been derived as in the ground-state case. For a meta-GGA, the TD-GKS potential thus depends on the TD density,

$$n(\mathbf{r}, t) = \sum_{k=1}^N |\varphi_k(\mathbf{r}, t)|^2, \quad (17)$$

on $\nabla n(\mathbf{r}, t)$, and on the TD kinetic energy density,

$$\tau(\mathbf{r}, t) = \frac{\hbar^2}{2m} \sum_{k=1}^N |\nabla \varphi_k(\mathbf{r}, t)|^2. \quad (18)$$

For ground state calculations with real orbitals, the kinetic energy density is well defined. However, as discussed by Bates and Furche³¹ and Baer and Kronik,⁴⁶ questions arise for current carrying states and in time-dependent calculations.

A first issue is the gauge variance of $\tau(\mathbf{r}, t)$. This gauge variance is seen when one considers the gauge transformation,

$$\mathbf{A}_{\text{ext}}[\Lambda](\mathbf{r}, t) = \mathbf{A}_{\text{ext}}(\mathbf{r}, t) + \nabla\Lambda(\mathbf{r}, t), \quad (19)$$

$$v_{\text{ext}}[\Lambda](\mathbf{r}, t) = v_{\text{ext}}(\mathbf{r}, t) - \frac{\partial}{\partial t}\Lambda(\mathbf{r}, t), \quad (20)$$

of the external potentials using the real gauge function $\Lambda(\mathbf{r}, t)$. It leads to a time- and position-dependent phase in all GKS orbitals,

$$\varphi_k[\Lambda](\mathbf{r}, t) = \varphi_k(\mathbf{r}, t) \exp\left(-\frac{ie}{\hbar}\Lambda(\mathbf{r}, t)\right), \quad (21)$$

where i is the imaginary unit. All observables should be gauge-invariant, i.e., independent of $\Lambda(\mathbf{r}, t)$. Consequently, one expects the GKS potential to be gauge invariant. However, the kinetic energy density transforms as

$$\tau[\Lambda](\mathbf{r}, t) = \tau(\mathbf{r}, t) - e(\nabla\Lambda(\mathbf{r}, t)) \cdot \mathbf{j}_p(\mathbf{r}, t) + \frac{e^2}{2m}|\nabla\Lambda(\mathbf{r}, t)|^2 n(\mathbf{r}, t), \quad (22)$$

with the paramagnetic current density

$$\mathbf{j}_p(\mathbf{r}, t) = \frac{\hbar}{m} \sum_{k=1}^N \text{Im}[\varphi_k^*(\mathbf{r}, t) \nabla \varphi_k(\mathbf{r}, t)]. \quad (23)$$

As τ enters the GKS potential directly, gauge invariance of the GKS potential is not guaranteed.

A second problem arises in the continuity equation due to the non-multiplicative character of the potential (11): Starting from the time-dependent GKS equation,

$$i\hbar \frac{\partial}{\partial t} \varphi_k(\mathbf{r}, t) = \hat{h}_{\text{GKS}}(\mathbf{r}, t) \varphi_k(\mathbf{r}, t), \quad (24)$$

one can derive

$$\begin{aligned} \frac{\partial}{\partial t} |\varphi_k(\mathbf{r}, t)|^2 &= \frac{1}{i\hbar} \left[\varphi_k^*(\mathbf{r}, t) \hat{h}_{\text{GKS}}(\mathbf{r}, t) \varphi_k(\mathbf{r}, t) \right. \\ &\quad \left. - \varphi_k(\mathbf{r}, t) \hat{h}_{\text{GKS}}(\mathbf{r}, t) \varphi_k^*(\mathbf{r}, t) \right] \\ &= \frac{2}{\hbar} \text{Im} \left[\varphi_k^*(\mathbf{r}, t) \hat{h}_{\text{GKS}}(\mathbf{r}, t) \varphi_k(\mathbf{r}, t) \right], \end{aligned} \quad (25)$$

where the time-dependent GKS-Hamiltonian for meta-GGAs is

$$\hat{h}_{\text{GKS}}(\mathbf{r}, t) = -\frac{\hbar^2}{2m} \nabla^2 + v_{\text{local}}(\mathbf{r}, t) + v_{\tau}^{\text{GKS}}(\mathbf{r}, t), \quad (26)$$

with $v_{\text{local}}(\mathbf{r}, t) = v_{\text{ext}}(\mathbf{r}, t) + v_{\text{H}}[n](\mathbf{r}, t) + v^{\text{loc}}(\mathbf{r}, t)$. Inserting Eq. (26) with Eq. (11) into Eq. (25) leads to

$$\begin{aligned} \frac{\partial}{\partial t} |\varphi_k(\mathbf{r}, t)|^2 &= \frac{2}{\hbar} \text{Im} \left\{ \varphi_k^*(\mathbf{r}, t) \left[-\frac{\hbar^2}{2m} \nabla^2 \varphi_k(\mathbf{r}, t) + v_{\text{local}}(\mathbf{r}, t) \right. \right. \\ &\quad \left. \left. \times \varphi_k(\mathbf{r}, t) - \frac{\hbar^2}{2m} \nabla \cdot \left(\frac{\partial e_{\text{xc}}^{\text{mGGA}}}{\partial \tau} \nabla \varphi_k(\mathbf{r}, t) \right) \right] \right\} \\ &= -\nabla \cdot \left\{ \frac{\hbar}{m} \text{Im} \left[\varphi_k^*(\mathbf{r}, t) \nabla \varphi_k(\mathbf{r}, t) \right] \right. \\ &\quad \left. \times \left(1 + \frac{\partial e_{\text{xc}}^{\text{mGGA}}}{\partial \tau}(\mathbf{r}, t) \right) \right\}. \end{aligned} \quad (27)$$

Finally, summing over k yields

$$\frac{\partial n(\mathbf{r}, t)}{\partial t} = -\nabla \cdot \left[\mathbf{j}_p(\mathbf{r}, t) \left(1 + \frac{\partial e_{\text{xc}}^{\text{mGGA}}}{\partial \tau}(\mathbf{r}, t) \right) \right]. \quad (28)$$

Thus, the continuity equation no longer holds.

The gauge variance and the violation of the continuity equation can be addressed²¹ by replacing the kinetic energy density of Eq. (5) by

$$\hat{\tau}(\mathbf{r}, t) = \tau(\mathbf{r}, t) - m \frac{|\mathbf{j}_p(\mathbf{r}, t)|^2}{2n(\mathbf{r}, t)}, \quad (29)$$

as suggested by Becke⁵⁹ and Tao.²⁰ This correction also restores the property that $\hat{\tau}$ can be used to detect iso-orbital regions. Using this current density correction in TD-GKS, called ‘‘TD-CGKS,’’ means that one replaces all appearances of τ in the meta-GGA definition by $\hat{\tau}$. Doing so and taking the functional derivative with respect to the orbitals shows that $\hat{v}_{\tau}^{\text{GKS}}$ is replaced by

$$\hat{v}_{\tau}^{\text{CGKS}} = \frac{1}{2m} \hat{\pi}(\mathbf{r}, t) \frac{\partial e_{\text{xc}}^{\text{mGGA}}(n, \nabla n, \hat{\tau})}{\partial \hat{\tau}}(\mathbf{r}, t) \hat{\pi}(\mathbf{r}, t), \quad (30)$$

where

$$\hat{\pi}(\mathbf{r}, t) = \hat{\mathbf{p}} - m \frac{\mathbf{j}_p(\mathbf{r}, t)}{n(\mathbf{r}, t)}, \quad (31)$$

in which $\hat{\mathbf{p}} = -i\hbar\nabla$. As detailed in the supplementary material, this replacement restores the validity of the continuity equation for the total density. (We note in passing that for the individual orbital densities, the continuity equation only holds, ‘‘on average,’’ as also shown in the supplementary material, and we discuss suitable numerical representations of the GKS and CGKS operators there.)

Due to the inherently local Kohn–Sham potential, TDDFT calculations using meta-GGAs that were performed in the Kohn–Sham instead of the GKS approach⁴⁴ did not need to worry about the challenges that arise from the operator-potential Eq. (11). They were, however, limited to the Krieger–Li–Iafrate approximation. TDDFT calculations for meta-GGAs in the GKS scheme with the operator potential and including the current density correction have been performed by Bates *et al.*^{21,60} for the Tao–Perdew–Staroverov–Scuseria⁹ functional. They found the effect of the current density correction to be relatively small. Other TD-GKS meta-GGA calculations did not take the correction into account.⁶¹ As it is clear from Eqs. (28) and (31) that a more pronounced τ -dependence will lead to more pronounced effects, the development of meta-GGAs, such as TASK, which have a strong τ -dependence, and to some extent also $r^2\text{SCAN}$, calls for a re-evaluation of the importance of the current density correction. In the following, we, therefore, present a systematic comparison of excitation spectra calculated with and without the use of the current density correction. We here focus on just a few model systems for which accurate calculations can be performed and for which accurate reference data are available. The chosen systems, though few, nevertheless, span a range of paradigmatic electronic structures, from few electron diatomic molecules to conjugated aromatic molecules and organic semiconductors.

IV. TD-(C)GKS CALCULATIONS WITH THE META-GGA
TASK

A. Results for diatomic molecules

We first calculate the absorption spectra of the diatomic molecules Li_2 and CO , because for these small systems, all numerical parameters can be chosen to yield high accuracy and accurate reference results are available. Our calculations focus on TASKx, where “x” denotes that we are using exchange only without a correlation functional, because in this way, we can focus on the effect of the pronounced τ -dependence that is part of the construction strategy of the TASK meta-GGA for exchange. However, we also do an exemplary check of the effect of correlation. For ground-state energetics, reasonable accuracy is achieved by combining TASKx with the cc-functional of Ref. 19, i.e., a self-interaction corrected LDA correlation. However, for the closed shell systems that we study here, the cc energy correction vanishes, reducing to LDAc, and therefore, we use TASKx+LDAc in our TDDFT calculation.

Following Ref. 62, we choose a bond length of $2.1421a_0$ for carbon monoxide (CO). In a first set of calculations, we check the relative accuracy of our real-time real-space calculations using a pseudopotential with a core correction as described in Sec. II B in comparison with explicitly linearized all-electron TDDFT with different Gaussian basis sets as implemented in TURBOMOLE.⁶³ The real-time real-space calculations use the program package BTDFFT and the propagation evaluation as described in Ref. 31. Concerning TURBOMOLE, we note that discrepancies that we observed with earlier versions of TURBOMOLE disappeared after the recently made update.⁶⁰ As a guide to the eye, in the following, we plot schematic excitation spectra with a Gaussian broadening $\exp(-\hbar(\omega - \omega_0)/\eta)^2$, where $\eta = 0.025$ and $\hbar\omega_0$ is the excitation energy. Tables listing all the excitation energies that are discussed here and in the following are given in the supplementary material.

The upper panel of Fig. 1 shows the schematic spectra obtained for CO with TASKx calculated with BTDFFT and TURBOMOLE, in straightforward GKS TD calculations, i.e., without the current density correction. In BTDFFT, we used a grid spacing of $0.2a_0$ and a spherical grid of radius $15a_0$. Using a bigger grid of $22a_0$ changes the excitation energy by less than 0.01 eV. In TURBOMOLE, the results are noticeably influenced by the basis set, and with increasing size of the basis set, the excitation energy systematically shifts toward the value that we obtained with BTDFFT. The high sensitivity toward the basis set and requirement for a very large basis is in line with earlier findings reported in the context of Kohn–Sham linear-response calculations for CO .⁶⁴ We, therefore, strongly assume that the remaining small discrepancy between the TURBOMOLE and BTDFFT spectra is due to the different numerical representations and would vanish in calculations that could reach the numerical limits. The lower panel of Fig. 1, which shows the excitation energy for TASKx combined with LDA correlation, confirms these findings. The LDA correlation shifts the excitation energy up by ~ 0.1 eV, and the basis-set dependence in TURBOMOLE is a bit less pronounced, but qualitatively, the results are the same. Therefore, we do not discuss the combination with LDA correlation for other systems.

As we have thus established an estimate of the numerical accuracy for the excitation energies, we investigate in our next step the influence of the current density correction. Figure 2 shows the comparison of the results from our real-time real-space calculations

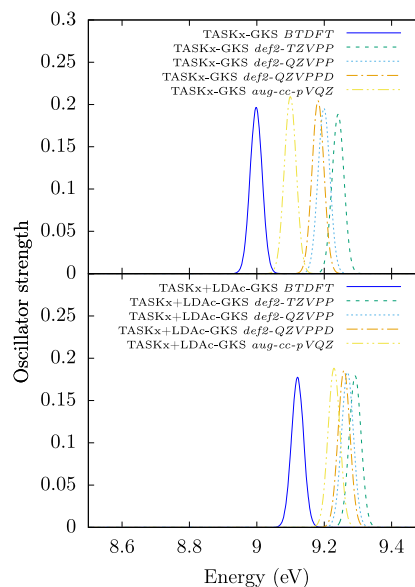


FIG. 1. Vertical excitation spectra calculated with BTDFFT and TURBOMOLE for CO calculated with TASKx-GKS in the upper panel and TASKx+LDAc-GKS in the lower panel.

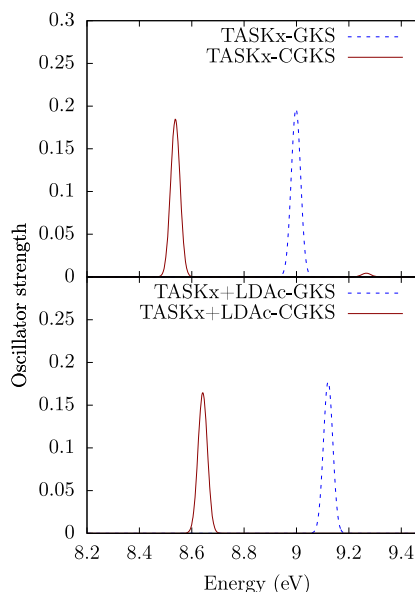


FIG. 2. Vertical excitation spectra for CO calculated with (CGKS) and without (GKS) the current density correction with TASKx in the upper panel and TASKx+LDAc in the lower panel.

without (dashed line) and with (solid line) the current density correction for TASKx (upper panel) and TASKx+LDAc (lower panel). The difference between GKS and CGKS is considerable, as the current density correction lowers the excitation energy by about 0.46 eV in both cases, shifting the excitation to 8.54 eV (TASKx) and 8.64 eV

(TASKx+LDAC).⁶⁵ This is an interesting observation in view of the experimental value of 8.51 eV for the first excitation energy in CO⁶⁶ and the third-order response coupled cluster (CC3) results of Ref. 62 that find the prominent excitation line at 8.47 eV (calculated with Dunning's basis set aug-cc-pVQZ⁶⁷): The current density correction obviously brings the TD-meta-GAA results in much better agreement with the reference data.

The second small molecule that we study as a test case is Li₂. For our calculations, we adopt the experimental bond length of 5.051 a₀ from Ref. 68. With a grid-spacing of 0.2a₀ and a grid radius of 15a₀, our real-time real-space calculations show two prominent excitation lines at 2.63 and 3.33 eV for TASKx-GKS, i.e., without the current density correction, as depicted in Fig. 3. In the TURBOMOLE calculations, we again observe a noticeable basis set dependence, in particular, for the second excitation. Whereas the TZVPP result deviates non-negligibly from the real-space real-time result for the second excitation, the QZVPP⁶⁹ and QZVPPD results are close to each other and to the real-time results. The remaining small discrepancy of 0.09 eV is in the range of what is to be expected on numerical grounds for such different techniques. With the aug-cc-pVQZ basis set, the second excitation shifts further in energy, but the calculation appears sensitive to numerical details and a previously unseen third excitation appears. We, therefore, regard the result with the QZVPPD basis set as the most reliable TURBOMOLE spectrum.

With the numerical trust range thus established, we again check the impact that the current density correction has on the spectra. Figure 4 shows the comparison of the spectra obtained with BTDFD for TASKx without (dashed line) and with (solid line) the current density correction. Again, we observe a substantial difference. The two prominent excitations are at 2.63 and 3.33 eV for TASKx-GKS and at 1.90 and 2.46 eV for TASKx-CGKS. Thus, the excitations shift by 0.73 and 0.87 eV, respectively.

Once more it is instructive to compare these values to reference data. We used the experimental and coupled cluster (CC3) results from Ref. 68 to calculate the respective values for the vertical excitation energies with the help of the harmonic approximation. This results in 1.86 and 2.57 eV for the experimental values and

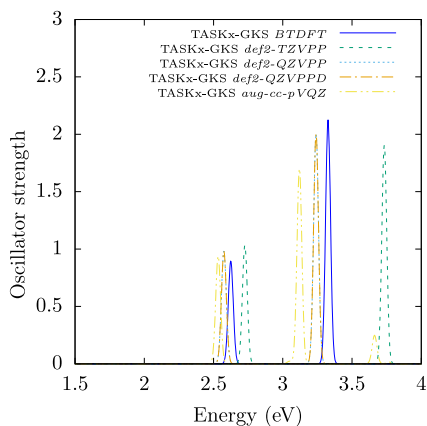


FIG. 3. Vertical excitation spectra calculated with BTDFD and TURBOMOLE for Li₂ calculated with TASKx-GKS.

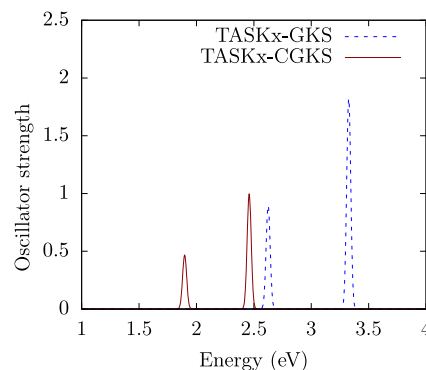


FIG. 4. Vertical excitation spectra for Li₂ calculated with (CGKS) and without (GKS) the current density correction with TASKx.

1.83 and 2.57 eV for the CC3 values. Therefore, taking the current density correction into account reduces the relative error significantly from 40.9% to 2.2% for the first excitation and from 29.6% to 4.3% for the second excitation, compared to the experimental data. Thus, the results for Li₂ confirm the previous findings for CO: The current density correction can have a large impact on the excitation energies, and the TASKx-CGKS results are in good agreement with the experimental and theoretical reference values.

B. Results for organic molecules

We continue our study with a few paradigm organic molecules that have a conjugated π -electron system and thus an electronic structure that shows other features than in diatomic molecules. Our first test case is benzene (C₆H₆), with Fig. 5 showing the schematic spectrum that we obtain with the real-space real-time approach without and with the current density correction. Again, the excitation shifts to a lower energy when going from GKS to CGKS. The magnitude of the shift, however, is with 0.15 eV smaller than what we observed for CO and Li₂. A possible explanation for this observation is seen in Eq. (28): It shows that the derivative $\partial e_{xc}^{mGGA}/\partial \tau$ is decisive for how strongly the continuity equation is violated, and this is also

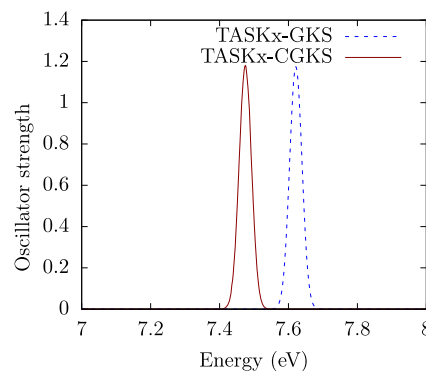


FIG. 5. Excitation spectrum of benzene (C₆H₆) calculated with TASKx-GKS and TASKx-CGKS. See the main text for discussion.

an indication for the strength of the current density correction that one expects. The importance of this derivative has also been pointed out in the context of meta-GGA calculations of the optical response of semiconductors.⁷⁰ It is one of the construction principles of TASK to generally have this derivative larger than previous meta-GGAs to increase the (ultra-)nonlocality of the meta-GGA exchange. However, the magnitude of this derivative for a given system depends on which values of n , s , and α are realized by the system's electronic structure and which parts of the enhancement factor are thus probed by the given system.⁴¹ Organic molecules, such as benzene, that have delocalized electrons are more "electron gas like" than a diatomic molecule. Consequently, one can expect that such molecules probe the enhancement factor closer to the electron-gas limit. Since both TASK and r^2 SCAN are designed to respect the electron gas limit, one expects a reduced derivative and thus a smaller impact of the current density correction, in agreement with the numerical observation.

We further note that in contrast to the energetic position of the excitations, for which we always observe a downshift, there does not seem to be a similarly systematic trend in the changes in the oscillator strengths of the main excitations: Whereas for CO and Li_2 , the oscillator strength of the dominant excitation decreased when going from GKS to CGKS, it slightly increases for benzene.

As a test case of a certain practical relevance, we next look at a model organic semiconductor molecule (NDI-1). In NDI-1, a naphthalene diimide core serves as an electron acceptor and two thiophene molecules are attached to it, one to the left and the other to the right, serving as electron donors. This system was designed with the aim of being used in organic solar cells, and it has been used in several TDDFT studies as a test case,^{44,71} because its lowest excitation is of charge-transfer character, with electron density being transferred from the thiophenes to the NDI core. This is the type of charge-transfer excitation that typically is of relevance in organic electronics, with a spatial separation of electron and hole densities, yet carrying some oscillator strength.

The NDI-1 molecule contains sulfur (S), which requires a pseudopotential with more than just 1s electrons in the core. Consequently, the core-correction described in Sec. II B cannot be used for S and we fall back to a regular Troullier–Martins pseudopotential for this atom (see the supplementary material for details), while using the core correction for all first-row atoms. To check whether this leads to inaccuracies, we calculated the GKS spectrum of NDI-1 also with all electrons using TURBOMOLE (spectra shown in the supplementary material). The two calculations agree closely. We are thus confident that for NDI-1, the pseudopotential inconsistency for the S atoms does not deteriorate the quality of the results.

Figure 6 shows the comparison of the result from the real-time real-space GKS and CKGS calculations. The first striking observation is that, now, the spectra with and without the current density correction are very similar. For TASKx-GKS, the first line appears at 2.05 eV, and for TASKx-CGKS, the first line appears at 2.03 eV, i.e., the difference is minute. Furthermore, it is instructive to compare the energy of the first peak, which corresponds to the above-mentioned charge-transfer excitation, with the energies that one obtains for this excitation with other xc approximations: With TD-LDA (and similarly with typical GGAs), this excitation is found at 1.69 eV, whereas an optimally tuned range-separated hybrid

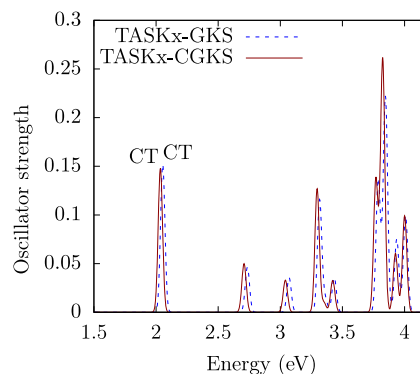


FIG. 6. Schematic excitation spectra for NDI-1 calculated without (GKS) and with (TASK-CGKS) the current density correction. The charge transfer excitation discussed in the main text is marked with "CT."

places it at 2.52 eV, close to the experimental result.⁷¹ Thus, this excitation paradigmatically shows the well-known problem that usual (semi-)local approximations severely underestimate charge-transfer excitation energies.⁷² In light of this comparison, the findings for TD-TASK appear as a mixed result: On the one hand, there is a clear improvement compared to TD-LDA, as about half of the gap between TD-LDA and the optimally tuned result is closed. This is plausible in view of the construction strategy of the TASK functional that stresses ultra-nonlocality and leads to field-counteracting terms.¹⁷ On the other hand, we see that the TD-TASK result is still noticeably lower than the optimally tuned reference, which shows that the TDDFT charge-transfer problem is not fully solved by TD-TASK.

These conclusions are confirmed by our last test, in which we calculate the excitations of two aggregated bacteriochlorophyll (BChl) chromophores, BChl-302 and BChl-303, from the B850 ring of the light harvesting complex 2 (LH2) of purple bacteria *Rhodoblastus (Rbl.) acidophilus*. This is a challenging test because one BChl molecule by itself shows two excitations, the so-called Q_y and Q_x excitations, but here, the two molecules are coupled. Consequently, one expects that there should be four excitations in the combined BChl-302 and BChl-303 system: The Q_y excitations typically show the characteristic J-aggregate type coupling, i.e., a symmetric and an antisymmetric coupling³¹ that leads to one excitation of high and one of low oscillator strength, and the Q_x excitations couple just weakly and mostly retain their individual molecular character. A calculation using the optimally tuned range-separated hybrid ω PBE, which we adapted from Ref. 73 and depict in the upper panel of Fig. 7, shows exactly these characteristics: There is one line of Q_y character with a high oscillator strength and one with low oscillator strength slightly below 1.8 eV, and the two Q_x excitations appear between 2.2 and 2.3 eV with a small energetic separation. The only further excitation in the shown energy range is a very weak line that appears above the coupled Q_x lines at 2.33 eV. A TD-LDA calculation, on the contrary, also shown in the upper panel, shows the characteristic problems that one has with spurious charge-transfer excitations in this system: Instead of two well-defined coupled Q_y excitations, there are now four excitations around 1.8 eV, because in addition to the two coupled Q_y lines, there are two low-lying

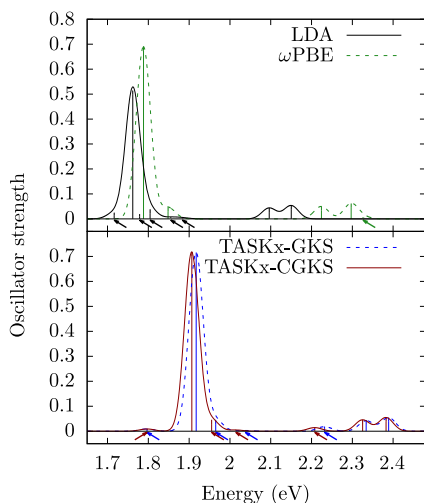


FIG. 7. Schematic excitation spectra for the combined BChl-302-BChl-303 molecular system calculated with LDA and ω PBE in the upper panel and TASKx-GKS and TASKx-CGKS in the lower panel. Excitations with very low oscillator strength that lie close to stronger excitations are additionally highlighted by small arrows below the energy axis.

spurious CT excitations. We marked the low-intensity excitations that lie close to the high-intensity ones by little arrows below the energy axis for clarity of the visualization, and the numerical values of all excitation energies can be found in the supplementary material.

The lower panel of Fig. 7 shows the TASKx results. As for NDI-1, the influence of the current density correction is negligible. In addition, as for NDI-1, the results with respect to the charge-transfer excitations are mixed: On the one hand, the coupling of the excitations is more correct than with the TD-LDA, as we observe the qualitatively correct picture of one high-strength and one low-strength excitation for the coupled Q_y and Q_x excitations. On the other hand, there are additional excitations slightly below 1.8 eV, at 2.04 eV, and at about 2.2 eV that are spuriously low, showing that the TDDFT charge-transfer problem is not fully fixed by TASKx.

V. TD-(C)GKS CALCULATIONS WITH THE META-GGA r^2 SCAN

A. Results for diatomic molecules

In the following, we investigate the importance of the current density correction for the r^2 SCANx functional by looking at the same paradigm test systems in Sec. IV. We again focus on only the exchange part in order to allow for a transparent comparison with the TASKx results, and also because the r^2 SCAN meta-GGA correlation is expected to have a τ -dependence of opposite sign to meta-GGA exchange,⁴¹ obscuring the non-locality effects in r^2 SCAN for x and c .

In the spectrum that we obtain for CO in GKS and CGKS with the real-time real-space propagation, we again observe a considerable difference between GKS and CGKS, similar to what we found for TASKx in Sec. IV B. The excitation is shifted by 0.36 eV from 8.82 eV (r^2 SCANx-GKS) to 8.46 eV (r^2 SCANx-CGKS), i.e., the shift

is smaller than for TASKx but still very noticeable. Once more taking the current density correction into account improves the agreement with the experimental reference.

The situation is similar for Li_2 . As for TASKx, we see a red shift of the excitation spectrum when switching from GKS to CGKS. The first excitation is shifted from 2.15 to 1.93 eV, and the second excitation is shifted from 2.76 to 2.49 eV. So again, the shift is noticeable but smaller than for TASK, and again, the current density correction improves the agreement with the experimental values of 1.86 and 2.57 eV. The oscillator strength shows a drop from GKS to CGKS for r^2 SCANx as well as for TASKx.

B. r^2 SCAN results for organic molecules

Turning toward the organic molecules, we again start with benzene. When going from r^2 SCANx-GKS to r^2 SCANx-CGKS, the dominant excitation line is once more red shifted but only by 0.07 eV from 7.24 to 7.17 eV, i.e., to a much lesser extent than for CO or Li_2 . The trend thus corresponds to the trend that is seen with the TASK functional, but the absolute scale is smaller. As discussed in Sec. IV B, these findings are explained by the fact that the magnitude of the current density correction is related to the electronic structure of the system, and the different meta-GGAs pick these differences up with different strengths, related to the different magnitude of $\partial e_x / \partial \tau$ in the different functionals.

Figure 8 shows the r^2 SCANx results for NDI-1, and again, we see the trend confirmed that we already saw for the TASK functional: There are only tiny differences between GKS and CGKS, i.e., the current density correction does not have any significant effect. With respect to the energy of the charge-transfer excitation, we observe some differences between r^2 SCANx-CGKS and TASKx-CGKS: With the former, the charge-transfer excitation shows up at 1.92 eV, whereas it is at 2.03 eV with TASKx. Thus, TASKx does somewhat better than r^2 SCAN in working against the spurious downshift of charge-transfer excitations that is common for semilocal functionals. This is in line with the construction strategy of TASK, which put emphasis on the ultra-nonlocality.

Finally, we look at the description of the coupling of the BChl-molecules of the combined BChl-302-BChl-303 system. The corresponding spectrum is shown in Fig. 9. One immediately sees that the effect of the current density correction is very small.

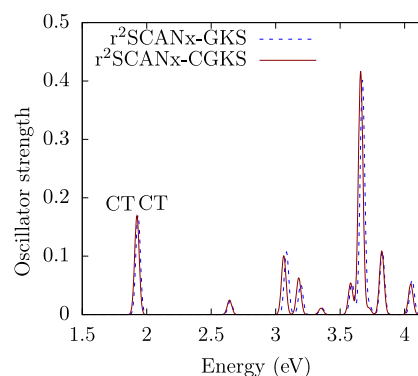


FIG. 8. Photoabsorption spectra for NDI-1 calculated with r^2 SCANx-GKS and r^2 SCANx-CGKS.

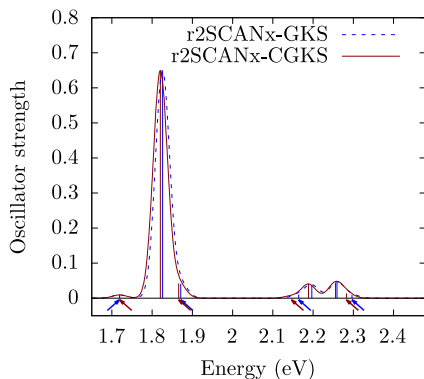


FIG. 9. Photoabsorption spectra for the combined BChl-302-BChl-303 molecules calculated with r^2 SCANx-GKS and r^2 SCANx-CGKS. The arrows indicate every single excitation. The arrows below the energy axis highlight the energetic positions of weak excitations that lie close to strong excitations and are thus hard to see.

In addition, the coupling of the Q_y excitations is similarly described with r^2 SCANx as with TASKx: There is one spurious low-strength excitation near the coupled Q_y -lines. The situation in the energy range of the Q_x excitations is more difficult with r^2 SCANx: Whereas for TASKx, one could identify the two coupled Q_x lines, as the spurious CT excitations were energetically separated from them, with r^2 SCANx, there are four excitations that lie so close to each other that one cannot count on the correct description of the coupling. So, overall, the results for r^2 SCANx are qualitatively similar to the ones obtained with TASKx, but the TASKx functional is doing somewhat better on the charge-transfer excitations. Both meta-GGAs, however, do not reach the accuracy of the tuned range-separated hybrid.

VI. SUMMARY AND CONCLUSION

We have calculated the absorption spectra of paradigm molecular model systems with the TASK and r^2 SCAN meta-GGA exchange functionals in the GKS scheme with and without a current density correction that restores gauge invariance and the continuity equation. The linear response was obtained by real-time propagation on a real-space grid, and we discussed how the reliability of pseudopotential results can be increased via a core-correction when meta-GGAs are used with usual norm-conserving pseudopotentials that have been constructed based on LDAs or GGAs.

Our results show that the current density correction can have a substantial influence on the excitations, changing the excitation energy by 40% and more than 0.8 eV in the most pronounced case of Li_2 . The current density correction shifts the excitations to lower energies and, in the cases studied here, improves the agreement with experiment. For larger conjugated organic molecules, however, we found that the correction is negligible. The differing importance of the current density correction is a consequence of differences in the electronic structure of the different molecules to which the meta-GGA enhancement factor is sensitive. That is, the magnitude of the current density correction is system dependent because different molecules probe different values of n , ∇n , and α , and these are

mapped to differing degrees of non-locality by the enhancement factor F of Eq. (1). The conjugated molecules have more delocalized densities than small molecules, such as CO and Li_2 , i.e., they are somewhat more “electron gas like.” TASK and r^2 SCAN respect the homogeneous electron gas limit and thus reduce their non-locality for systems that become closer to the electron-gas. As the magnitude of the current density correction is related to the degree of non-locality of the meta-GGA, one expects a reduced importance of the current density correction for systems with more delocalized, electron gas-like densities. It is, however, hard to *a priori* quantitatively predict the extent to which the non-locality of a meta-GGA is relevant in a given system. Furthermore, attempts to do so would require a very detailed analysis of the electronic structure, and while examples of such an analysis are known, e.g., in the context of understanding bandgaps,⁴¹ analyzing the interplay of the three variables n , ∇n , and α is not anything that one wants and can do routinely. Therefore, it is advisable not only for fundamental reasons but also for practical reasons to use the current density correction in all TDDFT calculations that employ meta-GGAs.

A comparison of TASKx and r^2 SCANx showed that the overall trends are very similar for the two functionals, but the effects of non-locality are more pronounced with TASKx than with r^2 SCANx. This is in line with the different non-empirical construction strategies of the two functionals, with r^2 SCAN focusing on ground-state energetics, while a special emphasis was given to the ultra-nonlocality in TASK. This reasoning also explains the somewhat better performance of TASKx for charge-transfer excitations. However, neither TASK nor r^2 SCAN reaches the quantitative accuracy for charge-transfer excitations that one sees in optimally tuned range-separated hybrid functionals. This finding is plausible and, to some extent, expected: The derivative discontinuity physics that TASK captures is necessary for a proper description of the field-counteracting term^{74,75} and charge-transfer, as repeatedly discussed in the past,^{17,72,76} yet other properties of a functional are also very important for the proper description of charge transfer excitations, especially being not or only weakly affected by self-interaction. Neither TASK nor r^2 SCAN is free from self-interaction, as their semilocal potentials cannot cancel the non-local self-Hartree potential. Designing a non-local self-interaction correction for meta-GGAs is thus a relevant direction of future research.

SUPPLEMENTARY MATERIAL

See the supplementary material for a detailed discussion of the continuity equation for meta-GGAs, the real-space representations of the GKS and CGKS operators, pseudopotential parameters, further numerical parameters and computational details, tables and figures listing further excitation details, comments on propagating SCANx, and the author contribution statement.

ACKNOWLEDGMENTS

We acknowledge the financial support by the Deutsche Forschungsgemeinschaft (DFG) under Grant No. KU 1410/4-1, the Elite Study Program “Biological Physics” of the Elite Network of Bavaria, and the Collaborative Research Network “Solar Technologies go Hybrid” from the Bavarian State Ministry of Science, Research, and the Arts.

AUTHOR DECLARATIONS

Conflict of Interest

The authors have no conflicts to disclose.

Author Contributions

Rian Richter: Conceptualization (supporting); Data curation (equal); Formal analysis (equal); Investigation (equal); Methodology (equal); Software (supporting); Validation (equal); Visualization (equal); Writing – original draft (equal); Writing – review & editing (supporting). **Thilo Aschebrock:** Conceptualization (supporting); Investigation (equal); Methodology (equal); Software (lead); Writing – original draft (equal); Writing – review & editing (supporting). **Ingo Schelter:** Software (supporting); Supervision (supporting); Validation (supporting); Writing – review & editing (supporting). **Stephan Kümmel:** Conceptualization (lead); Formal analysis (equal); Funding acquisition (lead); Investigation (equal); Methodology (equal); Project administration (lead); Resources (lead); Supervision (lead); Writing – original draft (equal); Writing – review & editing (lead).

DATA AVAILABILITY

The data that support the findings of this study are available within the article and its supplementary material. Raw numerical data are available from the corresponding author upon reasonable request.

REFERENCES

- L. Kronik, T. Stein, S. Refaely-Abramson, and R. Baer, “Excitation gaps of finite-sized systems from optimally tuned range-separated hybrid functionals,” *J. Chem. Theory Comput.* **8**, 1515–1531 (2012).
- S. Fürst, M. Haasler, R. Grotjahn, and M. Kaupp, “Full implementation, optimization, and evaluation of a range-separated local hybrid functional with wide accuracy for ground and excited states,” *J. Chem. Theory Comput.* **19**, 488–502 (2023).
- A. D. Becke, “Local exchange–correlation approximations and first-row molecular dissociation energies,” *Int. J. Quantum Chem.* **27**, 585–594 (1985).
- A. D. Becke, “Density-functional thermochemistry. IV. A new dynamical correlation functional and implications for exact-exchange mixing,” *J. Chem. Phys.* **104**, 1040–1046 (1996).
- A. D. Becke, “A new inhomogeneity parameter in density-functional theory,” *J. Chem. Phys.* **109**, 2092–2098 (1998).
- T. Van Voorhis and G. E. Scuseria, “A novel form for the exchange–correlation energy functional,” *J. Chem. Phys.* **109**, 400–410 (1998).
- J. P. Perdew, S. Kurth, A. C. V. Zupan, and P. Blaha, “Accurate density functional with correct formal properties: A step beyond the generalized gradient approximation,” *Phys. Rev. Lett.* **82**, 2544–2547 (1999).
- A. D. Boese and N. C. Handy, “New exchange–correlation density functionals: The role of the kinetic-energy density,” *J. Chem. Phys.* **116**, 9559–9569 (2002).
- J. Tao, J. P. Perdew, V. N. Staroverov, and G. E. Scuseria, “Climbing the density functional ladder: Nonempirical meta-generalized gradient approximation designed for molecules and solids,” *Phys. Rev. Lett.* **91**, 146401 (2003).
- K. Pernal, R. Podeszwa, K. Patkowski, and K. Szalewicz, “Dispersionless density functional theory,” *Phys. Rev. Lett.* **103**, 263201 (2009).
- Y. Zhao and D. G. Truhlar, “A new local density functional for main-group thermochemistry, transition metal bonding, thermochemical kinetics, and noncovalent interactions,” *J. Chem. Phys.* **125**, 194101 (2006).
- R. Peverati and D. G. Truhlar, “An improved and broadly accurate local approximation to the exchange–correlation density functional: The MN12-L functional for electronic structure calculations in chemistry and physics,” *Phys. Chem. Chem. Phys.* **14**, 13171–13174 (2012).
- J. Sun, B. Xiao, Y. Fang, R. Haunschuld, P. Hao, A. Ruzsinszky, G. I. Csonka, G. E. Scuseria, and J. P. Perdew, “Density functionals that recognize covalent, metallic, and weak bonds,” *Phys. Rev. Lett.* **111**, 106401 (2013).
- J. Sun, A. Ruzsinszky, and J. P. Perdew, “Strongly constrained and appropriately normed semilocal density functional,” *Phys. Rev. Lett.* **115**, 036402 (2015).
- H. S. Yu, X. He, and D. G. Truhlar, “MN15-L: A new local exchange–correlation functional for Kohn–Sham density functional theory with broad accuracy for atoms, molecules, and solids,” *J. Chem. Theory Comput.* **12**, 1280–1293 (2016).
- J. Tao and Y. Mo, “Accurate semilocal density functional for condensed-matter physics and quantum chemistry,” *Phys. Rev. Lett.* **117**, 073001 (2016).
- T. Aschebrock and S. Kümmel, “Ultranonlocality and accurate band gaps from a meta-generalized gradient approximation,” *Phys. Rev. Res.* **1**, 033082 (2019).
- J. W. Furness, A. D. Kaplan, J. Ning, J. P. Perdew, and J. Sun, “Accurate and numerically efficient r^2 SCAN meta-generalized gradient approximation,” *J. Phys. Chem. Lett.* **11**, 8208–8215 (2020).
- T. Lebeda, T. Aschebrock, and S. Kümmel, “First steps towards achieving both ultranonlocality and a reliable description of electronic binding in a meta-generalized gradient approximation,” *Phys. Rev. Res.* **4**, 023061 (2022).
- J. Tao, “Explicit inclusion of paramagnetic current density in the exchange–correlation functionals of current-density functional theory,” *Phys. Rev. B* **71**, 205107 (2005).
- J. E. Bates and F. Furche, “Harnessing the meta-generalized gradient approximation for time-dependent density functional theory,” *J. Chem. Phys.* **137**, 164105 (2012).
- K. Yabana and G. F. Bertsch, “Time-dependent local-density approximation in real time,” *Phys. Rev. B* **54**, 4484–4487 (1996).
- U. Saalmann and R. Schmidt, “Non-adiabatic quantum molecular dynamics: Basic formalism and case study,” *Z. Phys. D* **38**, 153–163 (1996).
- F. Calvayrac, P. Reinhard, and E. Suraud, “Spectral signals from electronic dynamics in sodium clusters,” *Ann. Phys.* **255**, 125–162 (1997).
- M. A. L. Marques, A. Castro, G. F. Bertsch, and A. Rubio, “Octopus: A first-principles tool for excited electron–ion dynamics,” *Comput. Phys. Commun.* **151**, 60–78 (2003).
- M. Mundt, S. Kümmel, R. van Leeuwen, and P.-G. Reinhard, “Violation of the zero-force theorem in the time-dependent Krieger–Li–Iaftrate approximation,” *Phys. Rev. A* **75**, 050501 (2007).
- K. Lopata and N. Govind, “Modeling fast electron dynamics with real-time time-dependent density functional theory: Application to small molecules and chromophores,” *J. Chem. Theory Comput.* **13**, 1355 (2011).
- W. Liang, C. T. Chapman, and X. Li, “Efficient first-principles electronic dynamics,” *J. Chem. Phys.* **134**, 184102 (2011).
- X. Andrade, D. Strubbe, U. De Giovannini, A. H. Larsen, M. J. T. Oliveira, J. Alberdi-Rodriguez, A. Varas, I. Theophilou, N. Helbig, M. J. Verstraete, L. Stella, F. Nogueira, A. Aspuru-Guzik, A. Castro, M. A. L. Marques, and A. Rubio, “Real-space grids and the octopus code as tools for the development of new simulation approaches for electronic systems,” *Phys. Chem. Chem. Phys.* **17**, 31371 (2015).
- J. J. Goings, P. J. LeStrange, and X. Li, “Real-time time-dependent electronic structure theory,” *WIREs Comput. Mol. Sci.* **8**, e1341 (2018).
- I. Schelter and S. Kümmel, “Accurate evaluation of real-time density functional theory providing access to challenging electron dynamics,” *J. Chem. Theory Comput.* **14**, 1910–1927 (2018).
- X. Li, N. Govind, C. Isborn, A. E. DePrince, and K. Lopata, “Real-time time-dependent electronic structure theory,” *Chem. Rev.* **120**, 9951–9993 (2020).
- J. Hekele, Y. Yao, Y. Kanai, V. Blum, and P. Kratzer, “All-electron real-time and imaginary-time time-dependent density functional theory within a numeric atom-centered basis function framework,” *J. Chem. Phys.* **155**, 154801 (2021).
- C. Shepard, R. Zhou, D. C. Yost, Y. Yao, and Y. Kanai, “Simulating electronic excitation and dynamics with real-time propagation approach to TDDFT within plane-wave pseudopotential formulation,” *J. Chem. Phys.* **155**, 100901 (2021).
- J. Mattiat and S. Lubner, “Recent progress in the simulation of chiral systems with real time propagation methods,” *Helv. Chim. Acta* **104**, e2100154 (2021).

- ³⁶G.-T. Bae and C. M. Aikens, "Time-dependent density functional theory study of the optical properties of tetrahedral aluminum nanoparticles," *J. Comput. Chem.* **43**, 1033–1041 (2022).
- ³⁷K. Yabana and G. F. Bertsch, "Time-dependent local-density approximation in real time: Application to conjugated molecules," *Int. J. Quantum Chem.* **75**, 55–66 (1999).
- ³⁸J. G. Brandenburg, J. E. Bates, J. Sun, and J. P. Perdew, "Benchmark tests of a strongly constrained semilocal functional with a long-range dispersion correction," *Phys. Rev. B* **94**, 115144 (2016).
- ³⁹Z. h. Yang, H. Peng, J. Sun, and J. P. Perdew, "More realistic band gaps from meta-generalized gradient approximations: Only in a generalized Kohn–Sham scheme," *Phys. Rev. B* **93**, 205205 (2016).
- ⁴⁰A. P. Bartók and J. R. Yates, "Regularized SCAN functional," *J. Chem. Phys.* **150**, 161101 (2019).
- ⁴¹T. Lebeda, T. Aschebrock, J. Sun, L. Leppert, and S. Kümmel, "Right band gaps for the right reason at low computational cost with a meta-generalized gradient approximation," *Phys. Rev. Mater.* **7**, 093803 (2023).
- ⁴²P. Borlido, J. Schmidt, A. W. Huran, F. Tran, M. A. L. Marques, and S. Botti, "Exchange-correlation functionals for band gaps of solids: Benchmark, reparametrization and machine learning," *npj Comput. Mater.* **6**, 96 (2020).
- ⁴³S. Kümmel and L. Kronik, "Orbital-dependent density functionals: Theory and applications," *Rev. Mod. Phys.* **80**, 3–60 (2008).
- ⁴⁴F. Hofmann and S. Kümmel, "Molecular excitations from meta-generalized gradient approximations in the Kohn–Sham scheme," *J. Chem. Phys.* **153**, 114106 (2020).
- ⁴⁵A. Seidl, A. Görling, P. Vogl, J. A. Majewski, and M. Levy, "Generalized Kohn–Sham schemes and the band-gap problem," *Phys. Rev. B* **53**, 3764–3774 (1996).
- ⁴⁶R. Baer and L. Kronik, "Time-dependent generalized Kohn–Sham theory," *Eur. Phys. J. B* **91**, 170 (2018).
- ⁴⁷M. Mundt and S. Kümmel, "Optimized effective potential in real time: Problems and prospects in time-dependent density-functional theory," *Phys. Rev. A* **74**, 022511 (2006).
- ⁴⁸H. O. Wijewardane and C. A. Ullrich, "Time-dependent Kohn–Sham theory with memory," *Phys. Rev. Lett.* **95**, 086401 (2005).
- ⁴⁹S.-L. Liao, T.-S. Ho, H. Rabitz, and S.-I. Chu, "Time-local equation for the exact optimized effective potential in time-dependent density functional theory," *Phys. Rev. Lett.* **118**, 243001 (2017).
- ⁵⁰T. Trepl, I. Schelter, and S. Kümmel, "Analyzing excitation-energy transfer based on the time-dependent density functional theory in real time," *J. Chem. Theory Comput.* **18**, 6577–6587 (2022).
- ⁵¹N. Troullier and J. L. Martins, "Efficient pseudopotentials for plane-wave calculations," *Phys. Rev. B* **43**, 1993–2006 (1991).
- ⁵²E. Engel, *Phys. Rev. B* **80**, 161205(R) (2009).
- ⁵³Y. Yao and Y. Kanai, "Plane-wave pseudopotential implementation and performance of scan meta-GGA exchange-correlation functional for extended systems," *J. Chem. Phys.* **146**, 224105 (2017).
- ⁵⁴A. Makmal, R. Armiento, E. Engel, L. Kronik, and S. Kümmel, "Examining the role of pseudopotentials in exact-exchange-based Kohn–Sham gaps," *Phys. Rev. B* **80**, 161204 (2009).
- ⁵⁵T. Schmidt and S. Kümmel, "One- and many-electron self-interaction error in local and global hybrid functionals," *Phys. Rev. B* **93**, 165120 (2016).
- ⁵⁶S. G. Louie, S. Froyen, and M. L. Cohen, "Nonlinear ionic pseudopotentials in spin-density-functional calculations," *Phys. Rev. B* **26**, 1738–1742 (1982).
- ⁵⁷A. Makmal, S. Kümmel, and L. Kronik, "Fully numerical all-electron solutions of the optimized effective potential equation for diatomic molecules," *J. Chem. Theory Comput.* **5**, 1731–1740 (2009).
- ⁵⁸A. Makmal, S. Kümmel, and L. Kronik, "Fully numerical all-electron solutions of the optimized effective potential equation for diatomic molecules," *J. Chem. Theory Comput.* **7**, 2665 (2011).
- ⁵⁹A. D. Becke, "Current density in exchange-correlation functionals: Application to atomic states," *J. Chem. Phys.* **117**, 6935–6938 (2002).
- ⁶⁰J. E. Bates, M. C. Heiche, J. Liang, and F. Furche, "Erratum: Harnessing the meta-generalized gradient approximation for time-dependent density functional theory," *J. Chem. Phys.* **156**, 159902 (2022).
- ⁶¹D. J. Tozer and M. J. G. Peach, "Molecular excited states from the scan functional," *Mol. Phys.* **116**, 1504–1511 (2018).
- ⁶²P.-F. Loos, A. Scemama, A. Blondel, Y. Garniron, M. Caffarel, and D. Jacquemin, "A mountaineering strategy to excited states: Highly accurate reference energies and benchmarks," *J. Chem. Theory Comput.* **14**, 4360–4379 (2018).
- ⁶³S. G. Balasubramani, G. P. Chen, S. Coriani, M. Diedenhofen, M. S. Frank, Y. J. Franzke, F. Furche, R. Grotjahn, M. E. Harding, C. Hättig, A. Hellweg, B. Helmich-Paris, C. Holzer, U. Huniar, M. Kaupp, A. Marefat Khah, S. Karbalaei Khani, T. Müller, F. Mack, B. D. Nguyen, S. M. Parker, E. Perlt, D. Rappoport, K. Reiter, S. Roy, M. Rückert, G. Schmitz, M. Sierka, E. Tapavicza, D. P. Tew, C. van Wüllen, V. K. Voora, F. Weigend, A. Wodyński, and J. M. Yu, "TURBOMOLE: Modular program suite for *ab initio* quantum-chemical and condensed-matter simulations," *J. Chem. Phys.* **152**, 184107 (2020).
- ⁶⁴F. Hofmann, I. Schelter, and S. Kümmel, "Linear response time-dependent density functional theory without unoccupied states: The Kohn–Sham–Sternheimer scheme revisited," *J. Chem. Phys.* **149**, 024105 (2018).
- ⁶⁵We also note that an additional excitation with low oscillator strength is seen in the TASKx-CGKS calculation at ~ 9.27 eV. Weak excitations at energies above the main excitation are also found in the other calculations, but they lie outside of the energy range shown in the figure.
- ⁶⁶E. S. Nielsen, P. Jørgensen, and J. Oddershede, "Transition moments and dynamic polarizabilities in a second order polarization propagator approach," *J. Chem. Phys.* **73**, 6238–6246 (1980).
- ⁶⁷T. H. Dunning, "Gaussian basis sets for use in correlated molecular calculations. I. The atoms boron through neon and hydrogen," *J. Chem. Phys.* **90**, 1007–1023 (1989).
- ⁶⁸M. Pecul, M. Jaszunski, and P. Jørgensen, "Singlet excitations and dipole polarizabilities of Li_2 , Li_3 and Li_4 clusters," *Mol. Phys.* **98**, 1455–1465 (2000).
- ⁶⁹F. Weigend, F. Furche, and R. Ahlrichs, "Gaussian basis sets of quadruple zeta valence quality for atoms H–Kr," *J. Chem. Phys.* **119**, 12753–12762 (2003).
- ⁷⁰V. U. Nazarov and G. Vignale, "Optics of semiconductors from meta-generalized-gradient-approximation-based time-dependent density-functional theory," *Phys. Rev. Lett.* **107**, 216402 (2011).
- ⁷¹A. Karolewski, T. Stein, R. Baer, and S. Kümmel, "Communication: Tailoring the optical gap in light-harvesting molecules," *J. Chem. Phys.* **134**, 151101 (2011).
- ⁷²D. J. Tozer, "Relationship between long-range charge-transfer excitation energy error and integer discontinuity in Kohn–Sham theory," *J. Chem. Phys.* **119**, 12697–12699 (2003).
- ⁷³I. Schelter, J. M. Foerster, A. T. Gardiner, A. W. Roszak, R. J. Cogdell, G. M. Ullmann, T. B. de Queiroz, and S. Kümmel, "Assessing density functional theory in real-time and real-space as a tool for studying bacteriochlorophylls and the light-harvesting complex 2," *J. Chem. Phys.* **151**, 134114 (2019).
- ⁷⁴S. J. A. van Gisbergen, P. R. T. Schipper, O. V. Gritsenko, E. J. Baerends, J. G. Snijders, B. Champagne, and B. Kirtman, "Electric field dependence of the exchange-correlation potential in molecular chains," *Phys. Rev. Lett.* **83**, 694–697 (1999).
- ⁷⁵A. Kaiser and S. Kümmel, "Revealing the field-counteracting term in the exact Kohn–Sham correlation potential," *Phys. Rev. A* **98**, 052505 (2018).
- ⁷⁶S. Kümmel, L. Kronik, and J. P. Perdew, "Electrical response of molecular chains from density functional theory," *Phys. Rev. Lett.* **93**, 213002 (2004).